Ag-Doped $BiVO_4$ Thin Films Deposited by Reactive Magnetron Sputtering as Visible Light Photocatalysts

Siavash Bakhtiarnia [a,b], Saeed Sheibani [a,*], Pascal Briois [b], Eric Aubry [b], Mohammad Arab Pour Yazdi [b]

a. School of Metallurgy and Materials Engineering, College of Engineering, University of Tehran, Tehran, Iran.

b. Institut FEMTO-ST, UMR 6174, CNRS, Univ. Bourgogne Franche-Comté, 15B, Avenue des Montboucons, 25030 Besançon, France

*Corresponding author at School of Metallurgy and Materials Engineering, University of Tehran, P.O. Box 11155-4563, Tehran, Iran. Tel.: +98 21 61114068; Fax: +98 21 88006076.

E-mail address: ssheibani@ut.ac.ir (S. Sheibani).

Abstract

In this study, the Ag-doped monoclinic $BiVO_4$ thin films were synthesized with a reactive magnetron sputtering technique and a post-annealing treatment. The X-ray diffraction and scanning electron microscopic analysis exhibited the formation of silver vanadate and metallic silver phase with various quantities depending on Ag loading. The photocatalytic experiments established the importance of Ag distribution in photoactivity enhancement since the heterojunctions between the phases are responsible for the charge separation. It was also proved that Ag-doping improves the photoactivity of monoclinic $BiVO_4$ at neutral pH by favoring the chromophore cleavage pathway in the photodegradation mechanism, which is a significant advantage over the pristine $BiVO_4$ being optimal at acidic pH.

Keywords: Photocatalyst; $BiVO_4$; Thin film; Sputtering; Rhodamine B.

1. Introduction

In recent years, bismuth vanadate in monoclinic scheelite structure (m-$BiVO_4$) has received an enormous amount of attention from the material scientific community thanks to its beneficial properties e.g. stability, non-toxicity, cheap production, optical absorption in the visible region, and the ability to decontaminate organic pollutions [1,2]. These properties enabled engineers to design procedures advancing photocatalytic processes using clean solar energy. There have been numerous attempts in synthesizing m-$BiVO_4$ through liquid-phase chemical routes, including sol-gel [3], hydrothermal [4], co-precipitation [5,6] that produce powder form, bringing certain downsides like recyclability, reusability, and using toxic chemicals, while the physical vapor deposition methods gained much less attention, particularly sputtering technique. Not only does it have advantages like clean low-cost products, and a high deposition rate [7], but they are also able to produce thin films that solve the recyclability problem making the entire photocatalytic water treatment more practical and economically viable. Magnetron sputtering technique has been widely used for high throughput stable and uniform productions in the industry [7], while few studies can be found in the literature utilizing this technique to synthesize $BiVO_4$ thin films.

Although there are a significant number of advantages in m-$BiVO_4$ thin films, it contains a few downsides like low charge mobility and electron recombination that should be overcome [8]. Doping and creating heterojunctions are the procedures that have been proved effective in solving the mentioned problems through charge separation preventing the photogenerated electrons to recombine [9,10]. Many elements were examined to enhance the photocatalytic properties of m-$BiVO_4$ e.g. Co [4], Cu [11], Ag [12], Mo [13], Se [14], Fe [15], Mo [16]. Amongst the dopant elements, silver shows promising prospects. Numerous researches have already stated the silver doping effectiveness in charge separation and narrowing the bandgap of TiO_2 [17]. It has also been

employed to enhance $BiVO_4$. Wang et al. synthesized $Ag^+/Ag/BiVO_4$ composite fibers and observed a redshift in the absorption spectrum and superior photocatalytic activity compared to the pristine $BiVO_4$ [18]. Xue et al. argued that Ag incorporation and formation of silver vanadate through a hydrothermal synthesis, affect the morphology and the heterojunction between the phases acts as a charge separator preventing the electron recombination, thus improving the photocatalytic properties of pure $BiVO_4$ [19]. Although many authors have also reported similar results utilizing various methods [20–23], to the best of our knowledge, there is no research on silver doping of $BiVO_4$ thin films using the sputtering technique.

This study aims to evaluate the effects of silver doping with various loadings on the photocatalytic activity enhancement of m-$BiVO_4$ by producing $Ag/BiVO_4$ thin films through a reactive magnetron sputtering technique on different substrates and experimenting with their photocatalytic potential in photodegradation of organic dyes at acidic and neutral pH. The structural, optical, and microscopic analysis give significant insights to the basic understanding of sputtered deposition of Ag-doped $BiVO_4$ thin films behavior for catalytic applications. The results were also compared with those of the pristine m-$BiVO_4$ thin films produced by reactive magnetron sputtering conducted by our team in previous research.

2. Experimental procedure

2.1. Thin film deposition

The deposition of $BiVO_4$ thin films was done by reactive DC magnetron sputtering technique using Bi, V, and Ag metallic targets (Ø 50 mm × 3 mm, purity 99.9 at. %) in argon-oxygen gas mixtures. A 90 L cylinder Alcatel 604 SCM (CIT Alcatel, Annecy, France) was used as the sputtering reactor vacuumed below 10^{-4} Pa via a turbo-molecular-pump. The chamber employs four circular planar with water-cooled magnetron sputtering sources while the rotating substrate

holder is parallel to the cathodes at 60 mm. The Bi and V cathodes were powered with a pulsed DC advanced energy dual generator and the silver doping was performed employing an Ag target supplied by a DC generator. The coating chemical compositions were controlled via adjusting the discharge power for the targets. The gas flow rates were adjusted with Brooks flowmeters and the sputtering pressure was measured with an MKS Baratron gauge. The specifications for the reactor used in reactive magnetron sputtering are presented elsewhere [24]. Glass, monocrystal silicon, and fused silica (76 ×26 × 1 mm^3) were mainly used as the substrates for measuring the film optical, structural, and photocatalytic properties. Before each sputtering process, the substrates were washed with alcohol and soap and then rinsed with water and placed on the substrate holder at a distance of 50 mm from the axis, which the substrate rotates. The deposition was performed at room temperature (no external heatings) and the sputtering pressure is controlled by the Ar flow rate. The parameters concerning the sputtering process are presented in Table 1.

Table 1. The sputtering parameters for the deposition of thin films.

Ar flow rate (sccm)	200	**Targets**	Bi	V	Ag
O_2 flow rate (sccm)	20	**Intensity (A)**	0.07 → 0.09	0.64 → 0.66	0.004 → 0.014
Total pressure (Pa)	4.5	**Power (W)**	9 → 11	247 → 255	1 → 4
Runtime (h)	3.5	**Frequency (kHz)**	70	50	-
Drawing distance (mm)	60	**T_{off} (μs)**	4	4	-

2.2. Characterization

X-ray characterization was performed by Bragg-Brentano XRD configuration using a BRUKER D8 focus diffractometer (Bruker AXS, Karlsruhe, Germany) with a cobalt X-ray tube (Co $K\alpha 1+\alpha 2$ radiations $\lambda_{\alpha 1}$ = 0.178897 nm and $\lambda_{\alpha 2}$ = 0.179278 nm) and equipped with a LynxEye

linear detector for structural analysis of the samples. The diffraction patterns were collected under airflow at a scan rate (2θ) of 0.1 degrees per second. The thickness of the thin films was measured using a step method with an Altysurf profilometer (Altisurf 500), manufactured by Altimet, equipped with a tungsten micro force inductive probe allowing an accuracy of about 20 nm. The calibration of the experimental device was realized with a reference sample number 787569 accredited by the CETIM organization prior to each measurement. For the morphology assessment, the top surface microscopic observations and the brittle-fracture cross-sections of the coatings as well as the determination of the film thickness were performed by a JEOL JSM 7800F FESEM. The chemical composition was analyzed by energy-dispersive X-ray spectroscopy (EDS, Bruker Nano, Berlin, Germany). The samples were carbon-coated prior to measurement to achieve sufficient electronic conductivity. The Bi and V atomic percentages are exclusively determined within the precision of the EDS measurements (the relative error is about 1 %) as EDS does not allow a precise estimation of the oxygen content in the films.

2.3. Photocatalytic performance measurement

The photocatalytic activity of the thin films was assessed through photodegradation of Rhodamine-B (RhB) solution (50 ml) with an initial concentration of 5 mg l^{-1} at acidic and neutral pH during 7 hours of illumination in the visible range by a xenon light source (150 W, Lot-Oriel) equipped with a UV-cutoff filter ($\lambda > 400$ nm) in a handmade setup. Hydrochloric was used to adjust the pH. The samples were fixed at a distance of 15 cm from the light source which emits constantly at 15 mW m^{-2} while placed in a water bath in order to keep the solution cool at room temperature (25 ˚C). The thin-film samples were placed in the solution 30 min prior to irradiation to reach the adsorption-desorption equilibrium. A 3 ml sample of the solution was collected every hour to determine its concentration by measuring the absorbance at 554 nm corresponding to the

maximum wavelength using a spectrophotometer (Libra S12-UV-visible (200-999 nm) - BIOCHROM). The kinetics of the photodegradation behaves based on the Langmuir-Hinshelwood model and described as follows (Eq. (1)) [25].

$$\ln \frac{C_0}{C} = k't \quad (1)$$

Here, C_0 is the initial concentration, t is the time of irradiation in visible light, C is the concentration of the solution at t, and k′ is the rate constant. The rate constant (k′) is achieved via plotting ln (C_0/C) as a function of t, whose slope corresponds to k′.

3. Results and discussion

Fig. 1 shows the correlation between the Ag atomic compositions of the thin films measured by the EDS, and the power discharge applied to the Ag target. The power discharges respecting Bi and V are kept in the range to achieve the stoichiometric ratio of 1. It is well known that the sputtering yield of Ag is very high, so with a minimum amount of power discharge (1w), the atomic percentage in the films exceeds 14% and continues to grow exponentially. To achieve lower amounts of Ag in the thin films, a various number of grids have been used to prevent the Ag atoms to reach the substrate. This might not be a desirable method since it may well have an unpredictable influence on the morphology. The exponential trend may be ascribed to the change in the spatial distribution of the plasma becoming more direct, which amounts to a higher diffusion of Ag particles to the substrate surface.

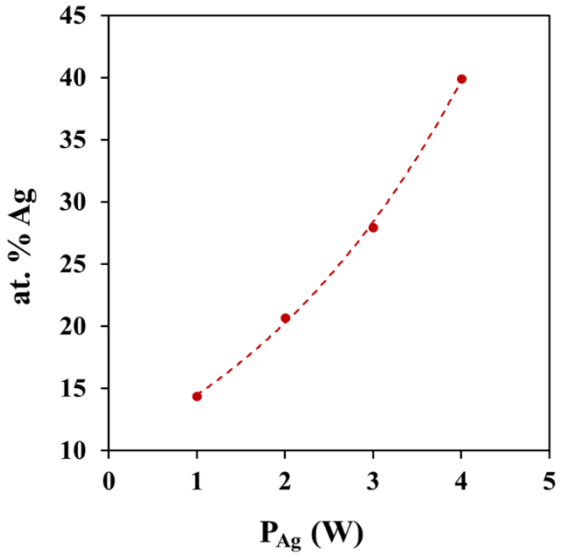

Fig. 1. (a) The atomic composition of Ag in the thin-film samples as a function of power discharge applied to the Ag target. (b) The EDS spectrum of Bi, V, Ag elements in a sample with a 24 Ag at. %

Fig. 2 (a) demonstrates the XRD diffractograms of the thin-film samples with various amounts of Ag at. % after 2h of annealing at 450 ˚C. The pristine sample only consists of the monoclinic phase (m-$BiVO_4$) (JCPDS No. 14-0688) with a small amount (≈ 3 %) of vanadium oxide (JCPDS No. 03-0207) calculated using the XRD peak intensity method. The presence of V_2O_5 is expected since the composition is slightly V-rich. The characteristic peak of AgO (JCPDS No. 76-1429) started to appear with introducing Ag at 3.5 and 8 %. It was expected to see a shift in the m-$BiVO_4$ peaks as a result of Ag dissolution but there was no apparent shift in the diffractograms (See Fig. 2(b)), which was also reported in the literature [26]. In the sample with a 21 Ag at. %, a marked change was observed as new phases emerged (≈ 37 %) which were recognized as Ag-V-O system called silver vanadate including $Ag_4V_2O_7$ (JCPDS No. 77-0097), and $AgVO_3$ (JCPDS No. 19-1153) whose characteristic peaks overlap at many 2θ that makes it difficult to distinguish the

phases considering the preferential orientations that happen in PVD processes. Fig 2 (c) illustrates the semi-quantification of the phases as a function of Ag at. %. The development of silver vanadate was continued by the addition of Ag up to at. 40 % except for the sample with 24 at. % Ag content that seems to enjoy the Ag in its metallic form (≈ 12 %) which its characteristic peak is observable at $2\theta = 45^{\circ}$.As the Ag at. % content of the thin films increases, the percentage of $BiVO_4$ decreases, indicating that vanadium forms a more thermodynamically favorable compound with Ag, leaving the bismuth to form Bi_2O_3 (≈ 1-14 %). In the sample with 40 at. % of Ag, the intensity of the peaks corresponding to m-$BiVO_4$ was significantly decreased compared to those of the silver vanadates which indicates that the silver vanadate now consists of the majority of phases (≈ 57 % as opposed to 16 % for m-$BiVO_4$).

Although some researchers reported the emergence of the tetragonal phase by introducing Ag [26], this phenomenon was not observed here.

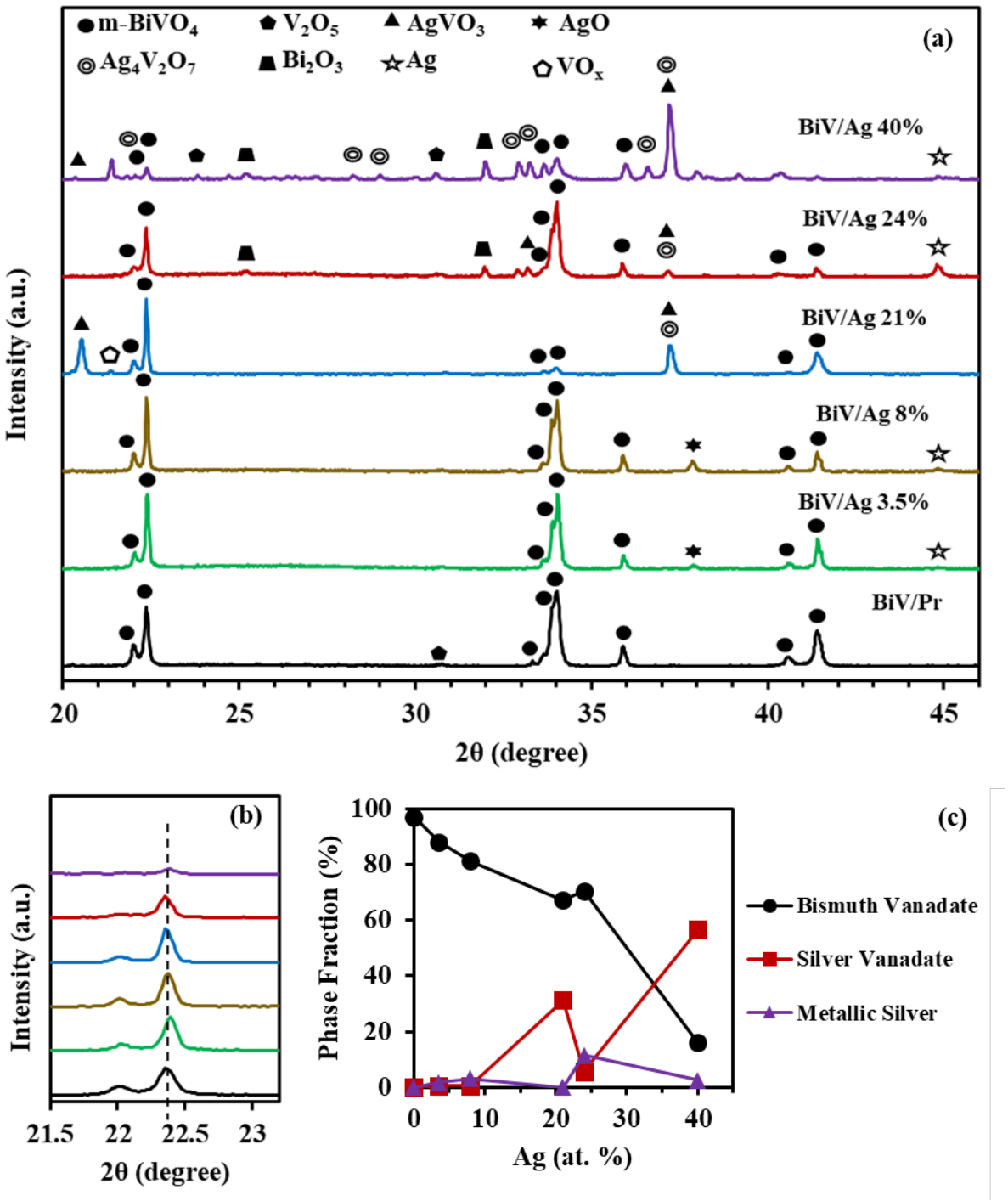

Fig. 2 (a) the diffractograms of thin films with various Ag at. %. (b) the diffractograms in the 21.5 – 23 2θ range, and (c) the relative fractional percentage of bismuth vanadate, silver vanadate, and Ag as a function of Ag at. %.

Fig. 3 depicts the top surface and brittle-fracture cross-sections of FESEM observations samples with the Ag content of (a) pristine as-deposited $BiVO_4$, (b) pristine $BiVO_4$ annealed at 450 ˚, (c) 3.5, (d) 8, (e) 21, (f) 24, (g) 28, (h) 40 at. %. It can be seen that in the as-deposited pristine $BiVO_4$ sample, the morphology dense and uniform with no apparent porosity in film, while the annealed sample developed cracks and porosity which suggests the occurrence during annealing. This phenomenon was discussed in detail in the previous work of our team (Ref – in press). A marked change in domain size is observable in the morphology of the samples with the Ag content compared to that of the pristine. The sample with 24 Ag at. % behaves differently with the significantly smaller domain sizes compared to other samples with Ag content. It can be concluded that the smaller domain size results in a higher interface between $BiVO_4$ and silver compounds which then intensifies the role of the heterojunction that prevents recombination through a more effective charge separation. It also amounts to a better chance for the photogenerated electrons and holes to reach the surface and contribute to photoreaction. The sample with 40 at. % of Ag has formed a mushroom-like morphology which seems to have an ideal distribution of phases throughout the surface obtaining a high interface of heterojunction that contribute to improving the photocatalytic activity. The cross-section observations of the samples also depict that the films have a dense structure with high porosity in some cases. The thickness of the samples is also measured at approximately one micrometer.

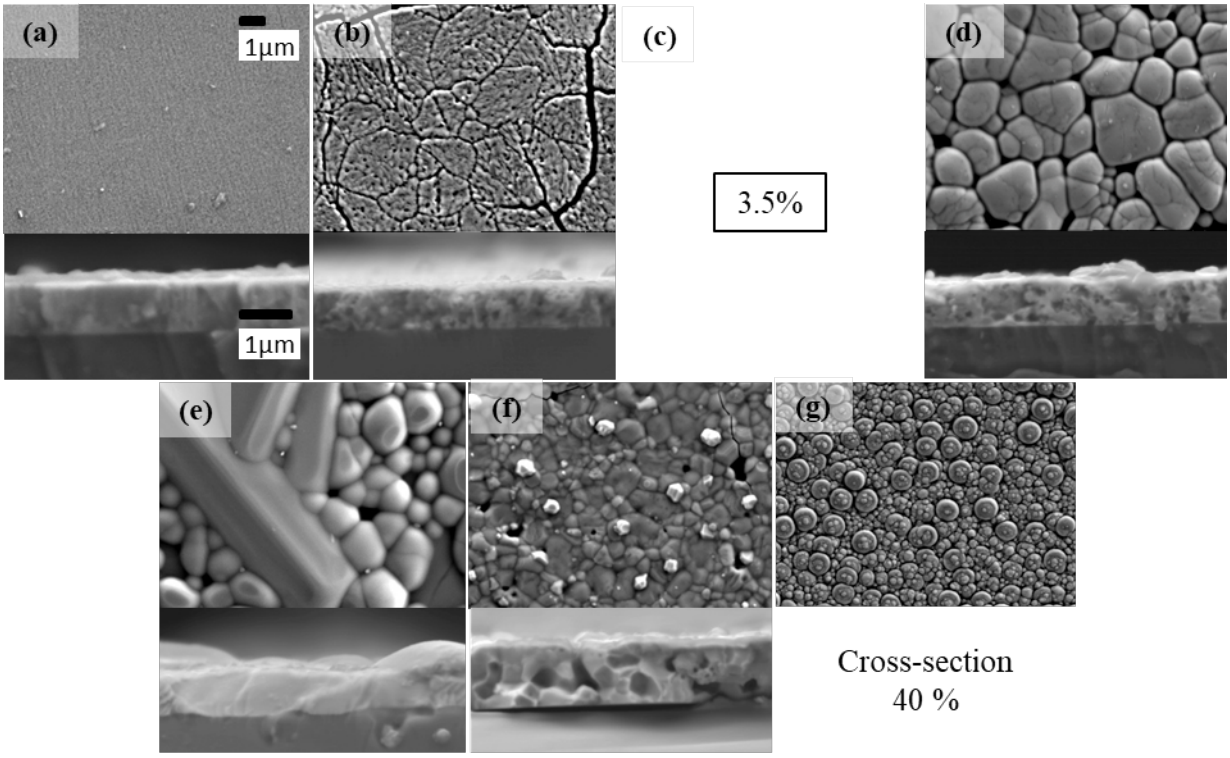

Fig. 3 FESEM observations of the top surface and brittle-fracture cross-sections of thin-film samples with the Ag content of (a) pristine as-deposited $BiVO_4$, (b) pristine $BiVO_4$ annealed at 450 ˚, (c) 3.5, (d) 8, (e) 21, (f) 24, (g) 28, (h) 40 at. %.

Fig.4 shows the mapping observations of samples with Ag content of (a) 8, (b) 21, (c) 24, (d) 28, (e) 40 at. %. The AgO particles in the sample with 8 at. % of Ag were uniformly dispersed in the $BiVO_4$ matrix, while poorly distributed silver vanadate in the shape of slabs in the sample with 21 at. % Ag was formed along with V_2O_5 in the form of little islands throughout the $BiVO_4$ matrix. The sample with 28 at. % of Ag behaved closely to the sample with 21 at. % except for the shape of silver vanadate which can be characterized as interconnected islands. It is also apparent that in the sample with 24 at. % of Ag, the small particles of silver oxide and silver vanadate were distributed uniformly over the surface which is ideal for photocatalytic applications as opposed to the thin films with 21 and 28 at. % of Ag where the silver is accumulated forming a slab-like

morphology which can result in little capability of charge separation of photogenerated electrons and holes. (further discussion with pristine and 40% mapping observations)

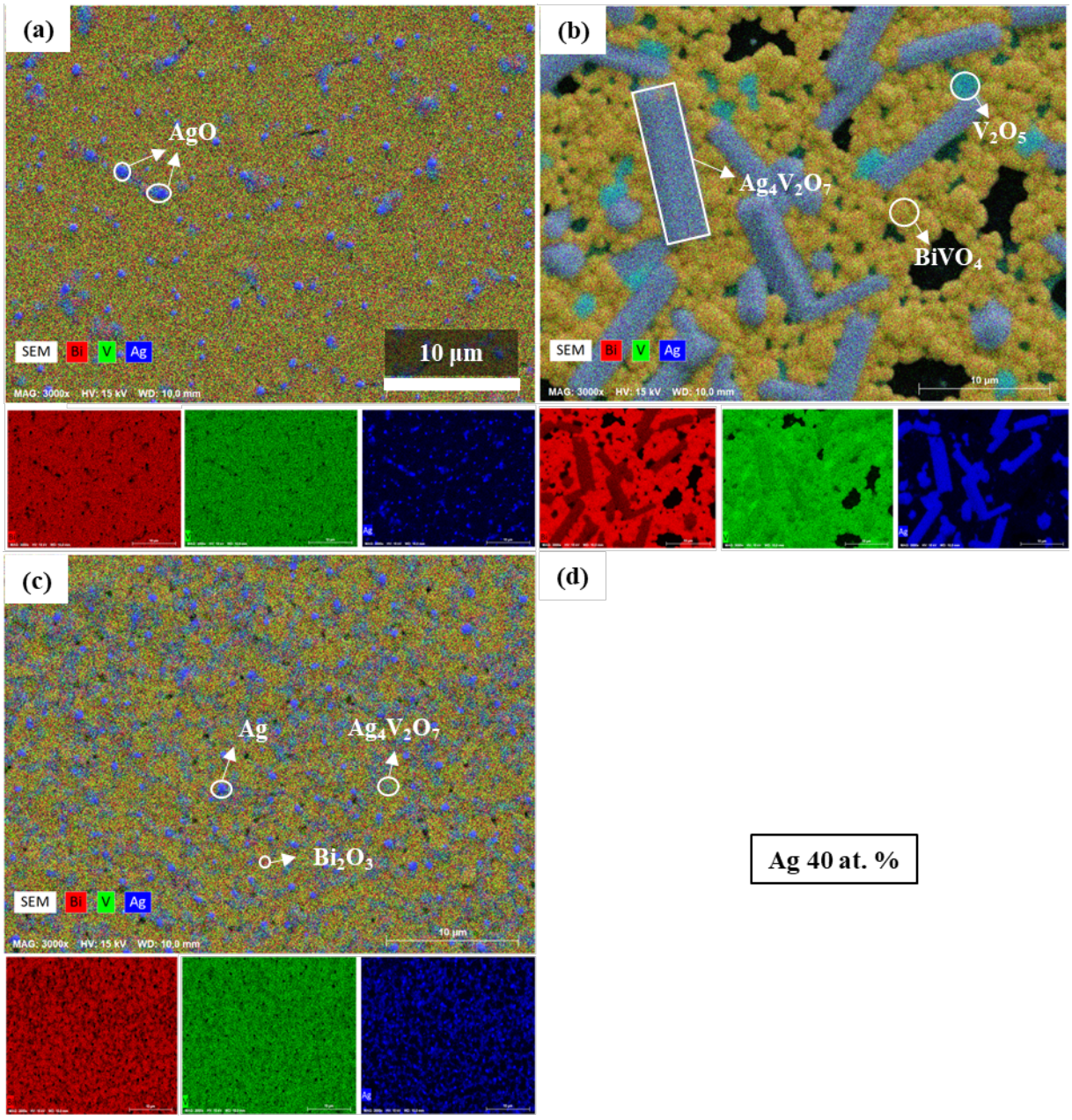

Fig. 4 Mapping observations of the thin-film samples with Ag content of (a) 8, (b) 21, (c) 24, (d) 28, (e) 40 at. %, and (f) pristine $BiVO_4$

Fig. 5 (a) illustrates the transmission spectra of the thin-film samples with different Ag content. The pristine sample shows an absorption edge near 520 nm while this value for the samples with Ag content is lower. The bandgaps of the thin films were obtained by extrapolation of the linear part of the $(\alpha h\nu)^n$ which is shown in Fig. 5 (b). Here n is equal to 2 assuming that $BiVO_4$ is a direct bandgap semiconductor. The bandgap value for the pristine sample is estimated at 2.45 eV while for the Ag content samples this value is around 2.5 eV except for the sample with 24 at. % which is significantly lower (1.65 eV). The reason for the higher bandgap value of the Ag content sample might be the formation of silver vanadate (Eg = 2.7 eV) which promotes a higher value of bandgap. This also agrees with the lower bandgap value for the sample with 24 Ag at. %, since the $Ag_2V_4O_7$ (silver vanadate) phase was less observed in this sample. Although the amount of Ag can have a significant impact on optical properties, it is not the only factor. The morphology, porosity, and structure should also be factored in to have a precise assessment.

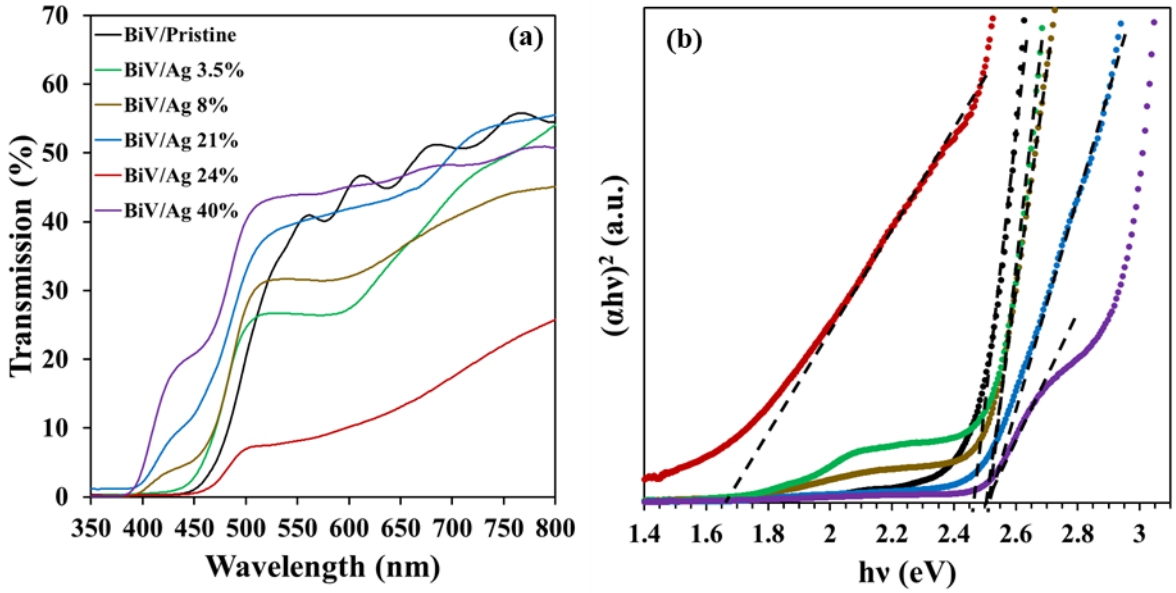

Fig. 5 (a) the transmission spectra of the thin-film samples with different Ag content. (b) bandgap values of the thin films using the Tauc plot.

Fig. 6 (a) exhibits the photodegradation of RhB solution at pH = 3 by $BiVO_4$ thin films doped with various silver loadings with a thickness of ≈ 1μm deposited on fused silica and annealed for 2 h at 450 ˚C. The inset graph shows the linear regression of $-\ln C/C_0$ against time in which the rate constant is extracted from its slope. The results of rate constants are presented in Fig. 6 (b). The highest photocatalytic performances were performed by the samples with 24 and 40 at. % of Ag that managed to photodegrade the RhB solution by 41 % and 44 % after 7 h of visible illumination, respectively. The other Ag-doped samples functioned at the 20-26 % range, which was slightly higher than that of the pristine sample (18 %). This proves the photoactivity enhancement of silver-doped $BiVO_4$ thin films. One can also conclude that over 24 % of Ag loading the enhancement stop improving. This lack of improvement by Ag loading is also observed from 8 to 21 at. % that can be ascribed to the poor distribution of silver over the surface by formation of oversize slab-like shape silver vanadate that results in low phase interface and limits the charge separation. This agrees with the previous microscopic observation in Fig. 3 and 4, which showed the best phase distribution concerning the sample with 24 at. % of Ag which has the highest photocatalytic activity.

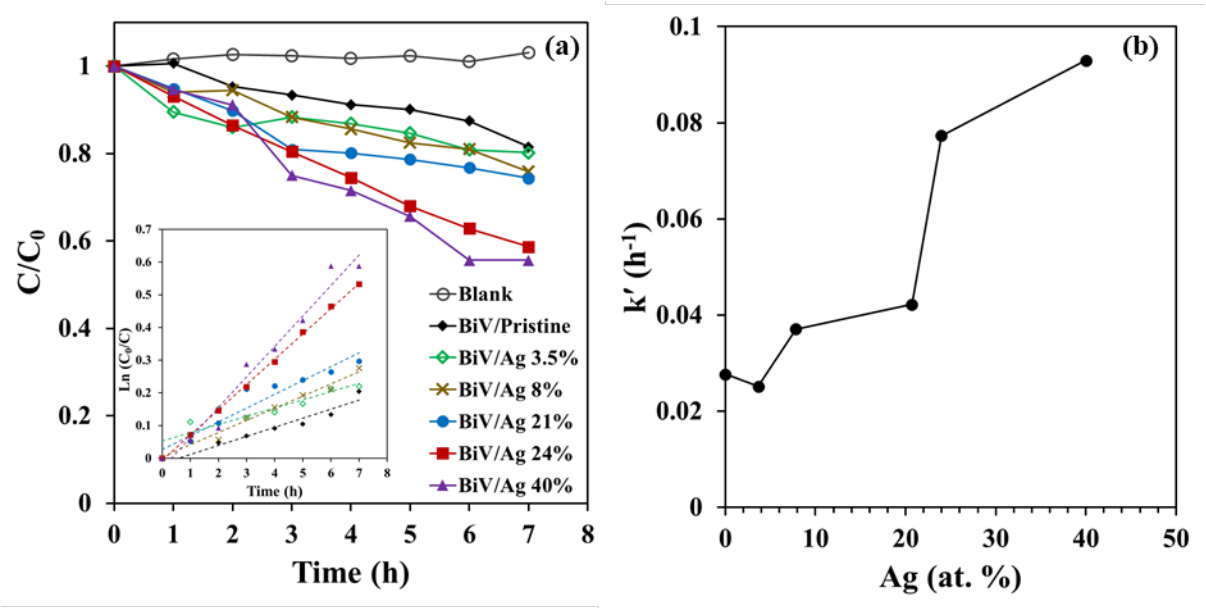

Fig. 6 (a) photodegradation of RhB by silver-doped $BiVO_4$ thin-film photocatalysts. (b) the rate constant of the photodegradation reaction as a function of silver content.

Fig. 7 (a) represents the photocatalytic degradation of RhB at different pH using thin-film photocatalysts deposited on different substrates (Fused silica and monocrystal silicon) with the same amount of silver content (24 %) annealed for 2h at 450 ˚C. Fig. 7 (b), (c), and (d) depicts the evolution of RhB degradation over incremental illumination time for the catalysts deposited on silicon at pH = 3, fused silica at pH = 3, and fused silica at pH = 7, respectively. It can be seen that the highest photodegradation is achieved at pH = 7, and the substrate nature did not affect photoactivity. It is in agreement with microscopic observations. Fig. 8 (a) shows the SEM top-surface and cross-section micrograms of the thin-film with 24 at. % of Ag deposited on monocrystal silicon and (b) depicts the mapping observations for the same sample. This figure exhibits that the morphology and elemental distribution of the sample with 24 at. % of Ag is identical on both silicon and fused silica (See Fig. 3 and 4) substrates. These experiments were conducted for comparison between the photocatalytic performance of silver-doped $BiVO_4$ and that

of the pristine $BiVO_4$ regarding substrate effect and photoreaction mechanism in different pH. This observation here contradicts the previous observations of our team for the pristine sample deposited on different substrates [ref: in press], which showed that the nature of the substrate can affect the reaction mechanism, and therefore the photocatalytic activity. The pristine $BiVO_4$ deposited on monocrystal silicon exhibited higher activity due to a change in morphology and light absorption efficiency, while apparently, the silver doping overshadows the effect of substrate nature. This argument is also valid for the pH effect which was proved to be dependant, showing higher activity in acidic pH with no shift in the spectra over time, while in neutral pH due to the deethylation pathway, a blue shift was observed and a reduction in photocatalytic potential. Here we can also observe that the silver-doped sample did not undergo the deethylation pathway, thus no blue-shift is seen. Therefore it is concluded that the photodegradation pathway of RhB by silver-doped $BiVO_4$ in both acidic and neutral pH is favored towards chromophore cleavage. So not only silver doping enhanced photoactivity through charge separation and electron mobility, but it also improved its photocatalytic activity in neutral pH independent of substrate nature, which is an important advantage for an economic design in the industry.

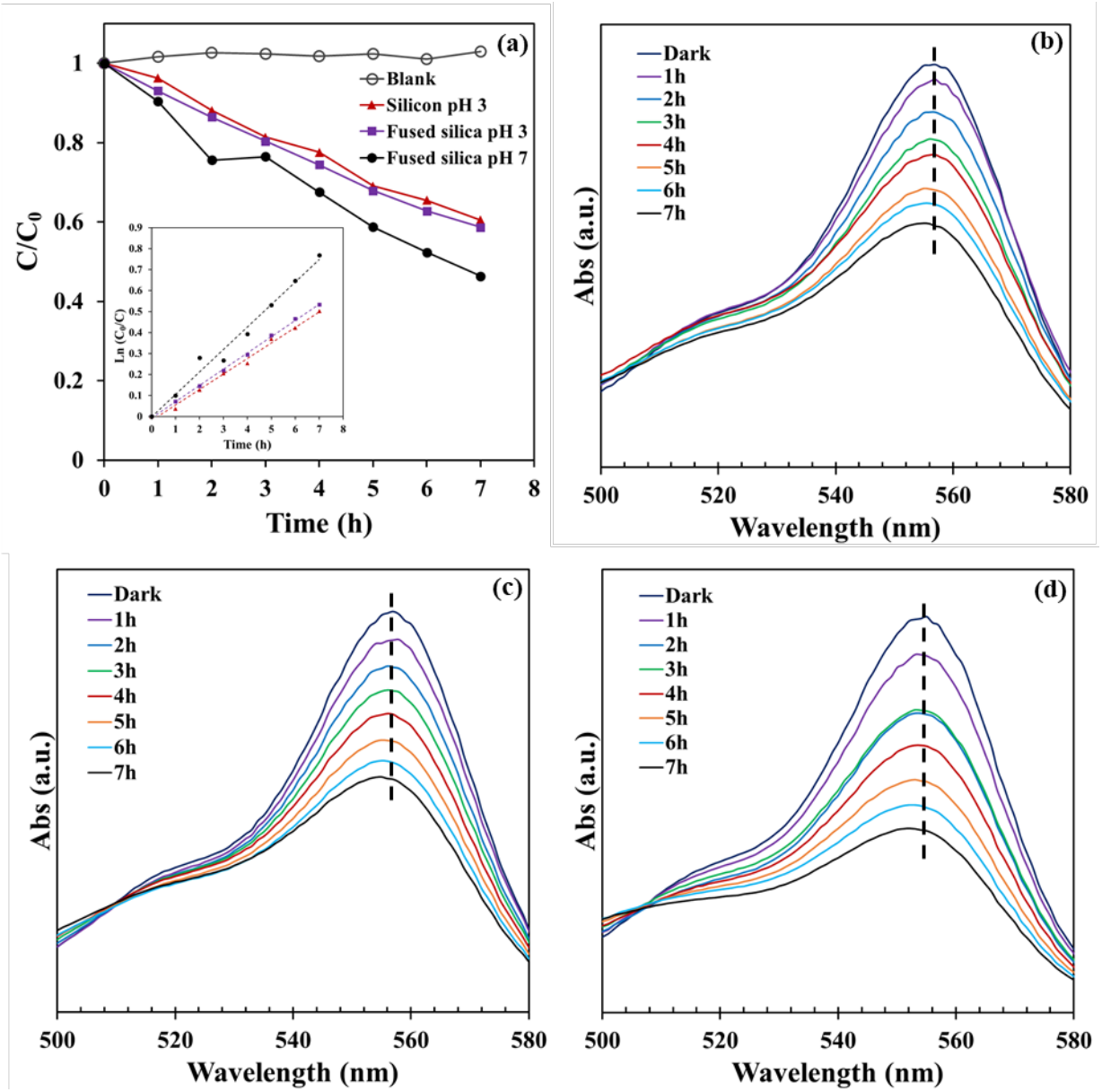

Fig. 7 (a) RhB photodegradation at different pH by the photocatalyst deposited on fused silica and monocrystal silicon with 24 at. % of Ag. (b), (c), and (d) illustrates the evolution of RhB solution spectra over various time of illumination for the catalysts deposited on silicon at pH = 3, fused silica at pH = 3, and fused silica at pH = 7, respectively.

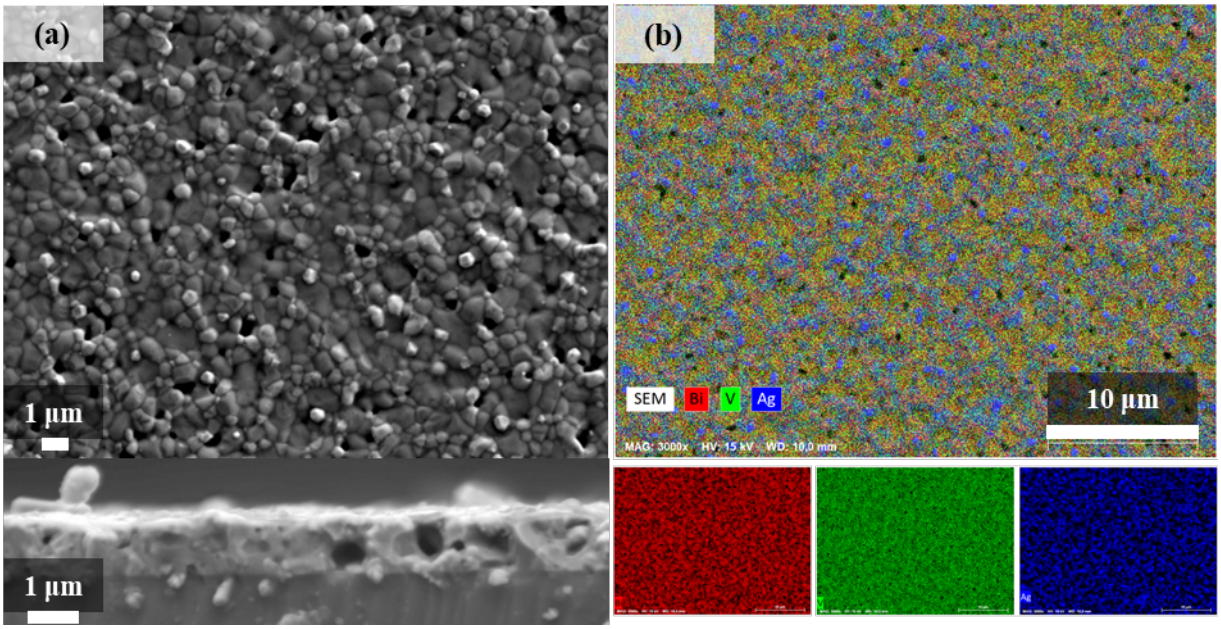

Fig 8 (a) SEM top-surface and cross-section micrograms of the thin-film with 24 at. % of Ag deposited on monocrystal silicon. (b) the separate elemental mapping observations for the same sample.

Conclusion

In this research, Ag-doped monoclinic $BiVO_4$ thin films were successfully deposited on fused silica and monocrystal silicon substrates using reactive magnetron sputtering technique and a post-annealing treatment for 2 h at 450 ˚C. The structural and microscopic analysis showed the formation of a silver vanadate phase as well as a metallic silver phase. The photodegradation of RhB solution as photocatalytic experiment proved the photoactivity enhancement by silver doping, and it was optimal when a sufficient distribution of silver is achieved. The sample with a 24 at. % of Ag managed to photodegrade the RhB solution by 41 % under 7 h of visible illumination. It was also established that the morphology and photoactivity enhancement of Ag-doped $BiVO_4$ thin films are independent of the substrate nature, unlike the pristine $BiVO_4$. In addition, it was proved that Ag-doped $BiVO_4$ thin-film photocatalysts are optimal in RhB photodegradation at neutral pH,

as opposed to the pristine $BiVO_4$ that showed the highest photocatalytic activity potential in acidic pH.

Conflict of interest

The authors declare that they have no conflict of interest.

Acknowledgments

The authors would like to acknowledge the supports of this study by the Iran National Science Foundation (project No: 98001285) and Pays de Montbéliard Agglomération.

Bibliography

[1] M.F.R. Samsudin, S. Sufian, B.H. Hameed, Epigrammatic progress and perspective on the photocatalytic properties of BiVO4-based photocatalyst in photocatalytic water treatment technology: A review, J. Mol. Liq. 268 (2018) 438–459. https://doi.org/10.1016/j.molliq.2018.07.051.

[2] A. Malathi, J. Madhavan, M. Ashokkumar, P. Arunachalam, A review on BiVO4 photocatalyst: Activity enhancement methods for solar photocatalytic applications, Appl. Catal. A Gen. 555 (2018) 47–74. https://doi.org/10.1016/j.apcata.2018.02.010.

[3] C. Yin, S. Zhu, Z. Chen, W. Zhang, J. Gu, D. Zhang, One step fabrication of C-doped BiVO4 with hierarchical structures for a high-performance photocatalyst under visible light irradiation, J. Mater. Chem. A. 1 (2013) 8367. https://doi.org/10.1039/c3ta11833a.

[4] Y. Geng, P. Zhang, N. Li, Z. Sun, Synthesis of Co doped BiVO4 with enhanced visible-light photocatalytic activities, J. Alloys Compd. 651 (2015) 744–748. https://doi.org/10.1016/J.JALLCOM.2015.08.123.

[5] R. Huo, X.L. Yang, Y.Q. Liu, Y.H. Xu, Visible-light photocatalytic degradation of glyphosate over BiVO4 prepared by different co-precipitation methods, Mater. Res. Bull. 88 (2017) 56–61. https://doi.org/10.1016/j.materresbull.2016.12.012.

[6] Synthesis and photocatalytic performances of BiVO4 by ammonia co-precipitation process - ScienceDirect, (n.d.). https://www-sciencedirect-com.ezproxy.utbm.fr/science/article/pii/S0022459608005422 (accessed January 10, 2021).

[7] S. Sarkar, N.S. Das, K.K. Chattopadhyay, Optical constants, dispersion energy parameters and dielectric properties of ultra-smooth nanocrystalline BiVO4 thin films prepared by rf-magnetron sputtering, Solid State Sci. 33 (2014) 58–66. https://doi.org/10.1016/j.solidstatesciences.2014.04.008.

[8] L. Ge, Novel visible-light-driven Pt/BiVO4 photocatalyst for efficient degradation of methyl orange, J. Mol. Catal. A Chem. 282 (2008) 62–66. https://doi.org/10.1016/J.MOLCATA.2007.11.017.

[9] B. Sun, G. Zhou, T. Gao, H. Zhang, H. Yu, NiO nanosheet/TiO2 nanorod-constructed p-n heterostructures for improved photocatalytic activity, Appl. Surf. Sci. 364 (2016) 322–331. https://doi.org/10.1016/j.apsusc.2015.12.158.

[10] A.A. Ismail, D.W. Bahnemann, Mesostructured pt/tio 2 nanocomposites as highly active photocatalysts for the photooxidation of dichloroacetic acid, J. Phys. Chem. C. 115 (2011) 5784–5791. https://doi.org/10.1021/jp110959b.

[11] M. Wang, P. Guo, T. Chai, Y. Xie, J. Han, M. You, Y. Wang, T. Zhu, Effects of Cu dopants on the structures and photocatalytic performance of cocoon-like Cu-BiVO4 prepared via ethylene glycol solvothermal method, J. Alloys Compd. 691 (2017) 8–14. https://doi.org/10.1016/J.JALLCOM.2016.08.198.

[12] X. Zhang, Y. Zhang, X. Quan, S. Chen, Preparation of Ag doped BiVO4 film and its enhanced photoelectrocatalytic (PEC) ability of phenol degradation under visible light, J. Hazard. Mater. 167 (2009) 911–914. https://doi.org/10.1016/j.jhazmat.2009.01.074.

[13] L. Chen, F.M. Toma, J.K. Cooper, A. Lyon, Y. Lin, I.D. Sharp, J.W. Ager, Mo-Doped BiVO 4 Photoanodes Synthesized by Reactive Sputtering, ChemSusChem. 8 (2015)

1066–1071. https://doi.org/10.1002/cssc.201402984.

[14] H. Ullah, A.A. Tahir, T.K. Mallick, Structural and electronic properties of oxygen defective and Se-doped p-type BiVO4(001) thin film for the applications of photocatalysis, Appl. Catal. B Environ. 224 (2018) 895–903. https://doi.org/10.1016/J.APCATB.2017.11.034.

[15] C. Regmi, Y.K. Kshetri, T.-H. Kim, R.P. Pandey, S.W. Lee, Visible-light-induced Fe-doped BiVO4 photocatalyst for contaminated water treatment, Mol. Catal. 432 (2017) 220–231. https://doi.org/10.1016/J.MCAT.2017.02.004.

[16] X. Yin, W. Qiu, W. Li, C. Li, K. Wang, X. Yang, L. Du, Y. Liu, J. Li, High porosity Mo doped BiVO4 film by vanadium re-substitution for efficient photoelectrochemical water splitting, Chem. Eng. J. 389 (2020) 124365. https://doi.org/10.1016/j.cej.2020.124365.

[17] S. Abbad, K. Guergouri, S. Gazaout, S. Djebabra, A. Zertal, R. Barille, M. Zaabat, Effect of silver doping on the photocatalytic activity of TiO2 nanopowders synthesized by the sol-gel route, J. Environ. Chem. Eng. 8 (2020) 103718. https://doi.org/10.1016/j.jece.2020.103718.

[18] K. Wang, L. Liang, H. Liu, X. Xie, Q. Hao, C. Liu, Facile synthesis of hollow and porous Ag+/Ag/BiVO4 composite fibers with enhanced visible-light photocatalytic performance, Mater. Lett. 161 (2015) 336–339. https://doi.org/10.1016/j.matlet.2015.08.145.

[19] Y. Xue, X. Wang, The effects of Ag doping on crystalline structure and photocatalytic properties of BiVO4, Int. J. Hydrogen Energy. 40 (2015) 5878–5888. https://doi.org/10.1016/j.ijhydene.2015.03.028.

[20] B. Zhou, X. Zhao, H. Liu, J. Qu, C.P. Huang, Synthesis of visible-light sensitive M-BiVO4 (M = Ag, Co, and Ni) for the photocatalytic degradation of organic pollutants, Sep. Purif. Technol. 77 (2011) 275–282. https://doi.org/10.1016/j.seppur.2010.12.017.

[21] M. Li, G. Xu, Z. Guan, Y. Wang, H. Yu, Y. Yu, Synthesis of Ag/BiVO 4 /rGO composite with enhanced photocatalytic degradation of triclosan, Sci. Total Environ. 664 (2019) 230–239. https://doi.org/10.1016/j.scitotenv.2019.02.027.

[22] A. Zhang, J. Zhang, Synthesis and characterization of Ag/BiVO 4 composite photocatalyst, Appl. Surf. Sci. 256 (2010) 3224–3227. https://doi.org/10.1016/j.apsusc.2009.12.009.

[23] L. Xu, Y. Wei, W. Guo, Y. Guo, Y. Guo, One-pot solvothermal preparation and enhanced photocatalytic activity of metallic silver and graphene co-doped BiVO 4 ternary systems, Appl. Surf. Sci. 332 (2015) 682–693. https://doi.org/10.1016/j.apsusc.2015.01.235.

[24] M.A.P. Yazdi, P. Briois, A. Billard, Influence of the annealing conditions on the structure of BaCe1-xYxO3-α coatings elaborated by DC magnetron sputtering at room temperature, Mater. Chem. Phys. 117 (2009) 178–182. https://doi.org/10.1016/j.matchemphys.2009.05.032.

[25] K.V. Kumar, K. Porkodi, F. Rocha, Langmuir-Hinshelwood kinetics - A theoretical study, Catal. Commun. 9 (2008) 82–84. https://doi.org/10.1016/j.catcom.2007.05.019.

[26] Y. Xue, X. Wang, The effects of Ag doping on crystalline structure and photocatalytic properties of BiVO4, Int. J. Hydrogen Energy. 40 (2015) 5878–5888. https://doi.org/10.1016/j.ijhydene.2015.03.028.